THE JOURNAL OF PHYSICAL CHEMISTRY C

Article

Cite This: J. Phys. Chem. C 2018, 122, 2747−2752

pubs.acs.org/JPCC

Emergence of Pendular and Rotary Motions of a Centimeter-Sized Metallic Sheet under Stationary Photoirradiation

Yugo Harada, Keisuke Koyoshi, Hiroki Sakuta, Koichiro Sadakane, Takahiro Kenmotsu, and Kenichi Yoshikawa*

Faculty of Life and Medical Sciences, Doshisha University, Kyotanabe 610-0321, Japan

Supporting Information

ABSTRACT: We report that both rhythmic pendular motion and rotary motion are generated under stationary irradiation by a green laser for a centimeter-sized metallic sheet floating on an aqueous solution. For a hammer-shaped aluminum sheet, regular pendular motion is caused by CW laser irradiation when the "handle" of the pendulum is in contact with the wall of the glass containing vessel. This rhythmic pendular motion occurs as on/off switching from a stationary state with an increase in laser power. We discuss the mechanism of such stable pendular motion in terms of limit-cycle oscillation with the aid of phenomenological coupled differential equations, by incorporating the effects of a decrease in interfacial tension with an increase in temperature under laser absorption and of the dissipation of heat into the environment. Stable rotary motion of the metallic sheet was also generated, driven by stationary laser irradiation. The chirality of the rotary motion, either clockwise or anticlockwise, for the metallic object could be selected through the introduction of chiral symmetry breaking in its morphology.

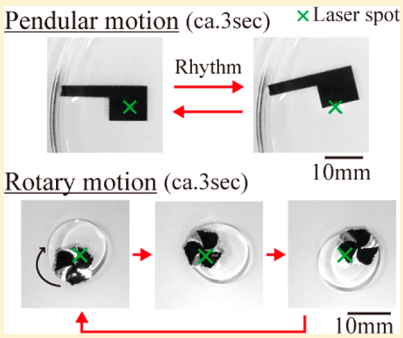

INTRODUCTION

Living organisms on earth maintain their lives under thermodynamically open conditions through the use of energy from the sun. There has recently been considerable interest in clarifying the mechanisms that underlie the emergence of regular motion in dissipative systems. Through recent studies on the self-propelled motion of both living organisms and artificial living material, it has become clear that irregular self-propelled motion can be converted to regular motion through the introduction of geometrical asymmetry.[1−6] For example, it was reported that the direction of translational motion is determined by the introduction of anterior−posterior asymmetry to either a chemical property or the physical structure of an object, and rotational motion is observed for an object with a rotationally asymmetric shape.[7−11] Furthermore, the emergence of regular motion in self-propelled particles through spontaneous symmetry breaking has attracted increasing interest, with regard to both physics and biology.[12−16]

In the present study, we focused on the motion induced by the instability of a solid/liquid interface, i.e., a spatiotemporal change in the interfacial free energy or interfacial tension. It is well-known that a spatial gradient of interfacial tension due to a thermal or chemical inhomogeneity at the interface can generate macroscopic agitation. This agitation can cause liquid flow known as Marangoni flow.[17−19] Interestingly, it has been reported that the macroscopic motion of a droplet or bubble can be induced accompanied by Marangoni instability or interfacial instability, under stationary dissipative conditions, including the experimental systems with photoirradiation.[20−32] Here, we study the generation of regular motion on a metallic sheet induced by Marangoni convection under local heating with a spatially fixed CW laser. We found that with a change in the magnitude of irradiating laser power a hammer-shaped object undergoes periodic pendular motion. In addition, a metal sheet entrapped with an oil droplet undergoes regular rotational motion, where the direction of rotation is determined by the geometric symmetry of the sheet.

EXPERIMENTAL METHODS

An aluminum (Al) sheet with a thickness of 11 μm was obtained from Toyo Al Echo Products Co., Ltd. (Japan; Foil Roll Black for Broiling Potatoes). Oleic acid was purchased from Nacalai Tesque (Tokyo, Japan). A CW laser (532 nm) was obtained from OXIDE Co. (Tokyo, Japan; LS03TT-M01). Experiments were performed at a room temperature of 18 °C. The motion of the Al sheet was captured by a digital video camera (Panasonic Co., Osaka, Japan; HC-600M) and a thermal camera (FLIR Systems Japan, Tokyo, Japan; FLIR T420). The recoded motion of the Al sheet was analyzed using ImageJ and Kinovea image-analysis software. To ensure that photons were absorbed effectively, we used the black-painted side of the Al sheet for the experiments. For the experiments on the generation of selective rotary motion (see Figures 5 and 6), we coated the surface of the Al sheet with black paint containing carbon black and poly(methyl methacrylate-*co*-butyl methacrylate) (Tamiya Ink Co., Japan; TS-14).

Received: November 10, 2017
Revised: December 26, 2017
Published: January 16, 2018

DOI: 10.1021/acs.jpcc.7b11123
J. Phys. Chem. C 2018, 122, 2747−2752

RESULTS AND DISCUSSION

Figure 1 shows pendular motion under irradiation by a laser at a spatially fixed position. The Al sheet was hammer-shaped, as

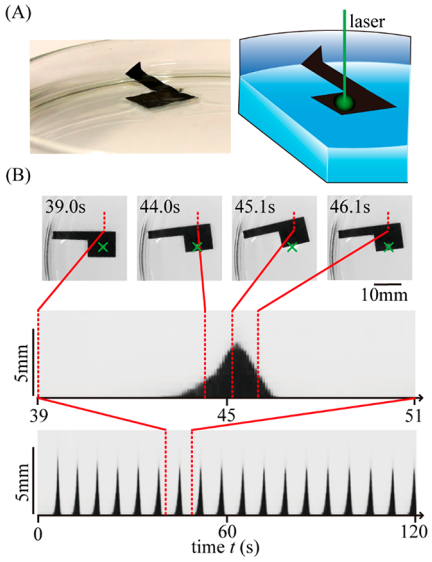

Figure 1. Pendular motion of a hammer-shaped aluminum sheet. (A) Photograph and schematic representation of the experimental system, where a hammer-shaped black aluminum (Al) sheet is floating on an aqueous phase. (B) Bottom: spatiotemporal diagram of pendular motion, where $t = 0$ corresponds to the initiation of laser irradiation. Middle: expansion of time axis on the spatiotemporal diagram. Top: images of the motion of the hammer-shaped object, where the green cross indicates the position of the laser spot.

shown in Figure 1A. In the experiment, the end of the "handle" of the hammer-shaped sheet was bent at a right angle to form a small triangle, as depicted in Figure 1A, which was positioned to be parallel to the wall of the experimental container. Figure 1B shows snapshots and spatiotemporal diagrams of the pendular motion of the object under stationary laser irradiation at a laser power of 0.45 W. The lower panel of Figure 1B shows a spatiotemporal diagram of the rhythmic pendular motion, where the middle panel shows a time expansion of the diagram for rhythmic motion. The spatiotemporal diagram indicates that the object maintains its pendular motion under stationary laser irradiation, and the period of this motion is on the order of 3 s.

Figure 2 shows the dependence of the pendular motion on laser power; Figure 2A exemplifies the time-dependent change in the angle $\Delta\theta$ $(= \theta - \theta_0)$ of laser-induced motion of the hammer-shaped object. Figure 2B shows a definition of the angle θ. The amplitude of the curve on the vertical axis of Figure 2A is the change in θ from its initial value θ_0 ($\theta_0 \approx 1/30$ rad). In these experiments, we set the initial condition so that the handle of the hammer-shaped object was in contact with the wall of the container. Figure 2C shows how the mode of movement of the object varies with the laser power: (i) stationary state without any moment (0−0.37 W) and (ii) rhythmic motion (0.37−0.5 W). Above a power of 0.5 W, the object again entered a stationary state without rhythmic motion. The transition from stationary to rhythmic states at a power of around 0.35 W was abrupt or discrete, as shown in Figure 2C.

Figure 3A shows the temperature distribution around the object as observed by an IR thermometer after 0.7, 6.2, 6.7, and

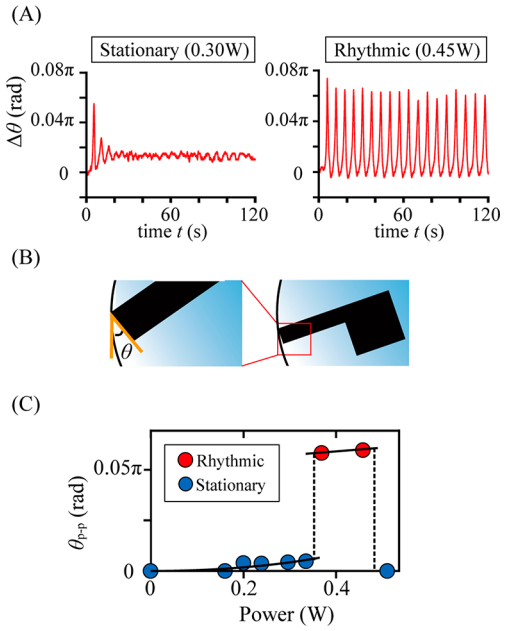

Figure 2. (A) Time-dependent change in the contact angle ($\Delta\theta$), just after the start of laser irradiation, for the motion of a hammer-shaped Al sheet. (B) Schematic illustration to show the change in angle θ. (C) Bifurcation diagram of the dynamic behavior of the hammer-shaped object, depending on the laser power. θ_{p-p} corresponds to the peak-to-peak amplitude of $\Delta\theta$ in (A). With an increase in laser power, the mode changes from "stationary" to "rhythmic". With a further increase in power, the object is repelled away from the laser focus and attaches to the periphery of the glass vessel in a stationary manner.

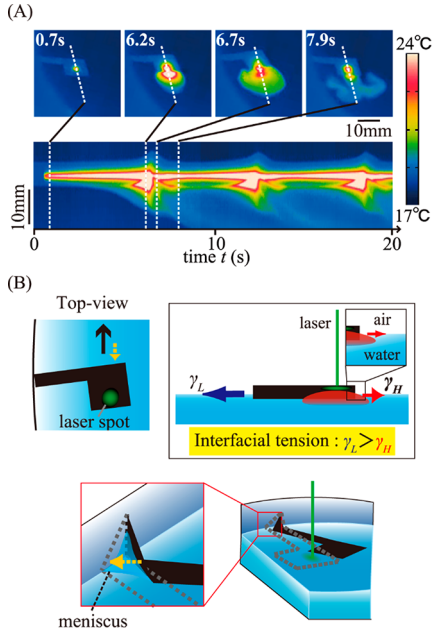

Figure 3. (A) Spatiotemporal diagram of the temperature profile for the rhythmic motion of the hammer-shaped object, together with snapshots of the spatial temperature profile. (B) Schematic representation of the difference in interfacial tension between the sides of the hammer-shaped plate under local heating by a laser. The black arrow shows the net force, and the light-orange arrow is the restoring force due to the meniscus.

7.9 s and the corresponding spatiotemporal diagram during rhythmic motion. The diagram clearly shows periodic heating

DOI: 10.1021/acs.jpcc.7b11123
J. Phys. Chem. C 2018, 122, 2747−2752

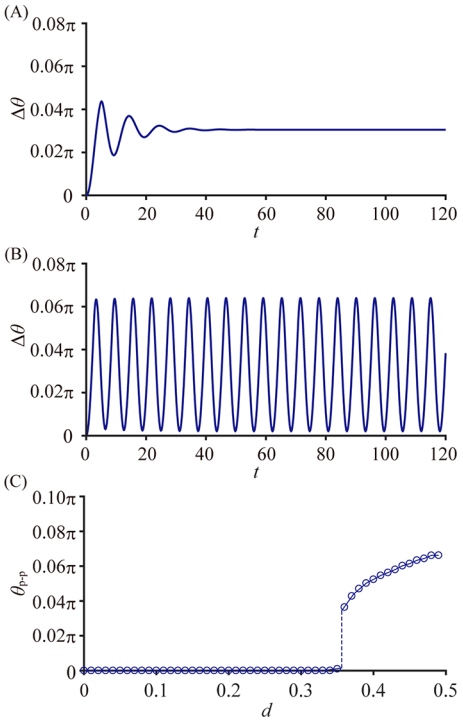

Figure 4. Results of the numerical simulation of pendular motion, by adapting the numerical eqs 1 and 2. (A) Damping motion to a stationary state when the laser power is weak, d = 0.3. (B) Rhythmic motion with a greater laser power, d = 0.45. (C) Dependence of the amplitude of rhythmic motion on the heating parameter, d. As for the details on the parametrizations, see the text. $\Delta\theta$ and θ_{p-p} correspond to those shown in (A) and (B), respectively.

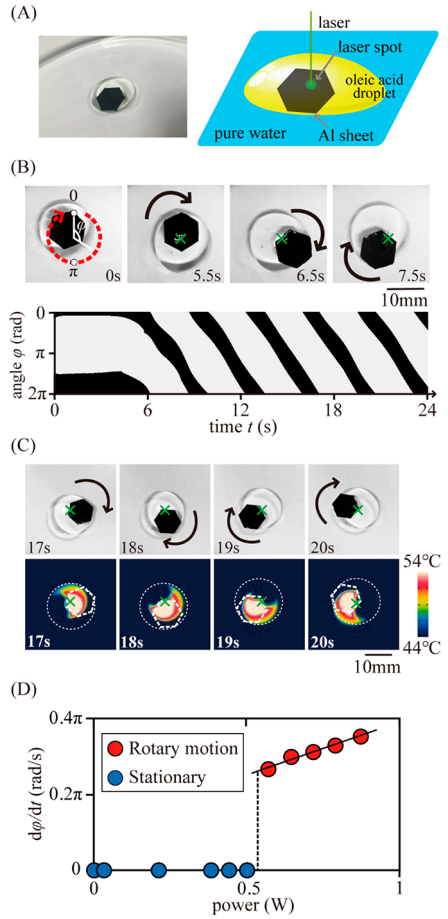

Figure 5. Rotary motion of a hexagonal Al sheet. (A) Photograph of the floating Al sheet entrapped inside an oil droplet (oleic acid, 260 μL) together with a schematic representation. (B) Example of rotary motion caused by CW laser irradiation and the corresponding spatiotemporal diagram. φ is defined as shown in the snapshot for 0 s. The direction of rotation is determined by the initial condition; i.e., the direction of rotation is bistable. (C) Snapshots of rotary motion and the corresponding temperature profiles. (D) Phase diagram of rotary motion dependent on the laser power.

of the hammer-shaped object coupled with periodic motion; i.e., movement of the object away from the laser spot is enhanced when the temperature of the object increased. On the basis of the above experimental results, we propose a mechanism for the pendular motion induced by laser irradiation, as shown in Figure 3B. It is well-known that a temperature gradient around a water/air interface leads to a gradient of interfacial tension in that area. This means that the tension at a lower temperature, γ_L, is greater than that at a higher temperature, γ_H. Because of this spatial gradient of the interfacial tension, the "head" of the hammer moves away from the region of higher temperature, as shown in Figure 3A. Another important factor in the periodic motion is the presence of a meniscus between the handle of the hammer and the glass vessel. When the hammer-shaped object moves away from the laser spot, the meniscus tends to make the object return to its initial position, like a spring. The competition between the driving force generated by laser irradiation and the restoring force exerted by the meniscus generates the observed pendular motion of the sample. Thus, the mechanism of pendular motion can be summarized as follows: First, the head of the hammer-shaped object moves due to laser irradiation while maintaining contact between the sample and the container wall. Next, the sample moves away from the focus of the laser due to the motion of the sample driven by laser irradiation. This means that the driving force of laser irradiation works by increasing the temperature of the sample. The restoring force exerted by the meniscus then returns the sample back to its initial position before laser irradiation. The competition between these forces leads to the pendular motion of the sample.

On the basis of the above results and discussion of pendular motion caused by laser irradiation, we propose a simple numerical model for this oscillatory motion. To express the essence of the mechanism of pendular motion, we use only two variables: θ, the angle of the long-axis of the hammer with respect to the wall of the outer vessel as shown in Figure 2B, and τ, the temperature normalized to room temperature. Using these two variables, we propose the following coupled differential equations.

$$\frac{d^2\theta}{dt^2} = -a\frac{d\theta}{dt} - b\theta + c\xi(\theta)\tau$$

$$\frac{d\tau}{dt} = d\xi(\theta) - e\tau \quad (1)$$

where a, b, c, d, and e are positive constants that depend on the arrangement of the experimental system. The first term on the right side of the upper equation in eq 1 shows the effect of viscous damping, and the second term is the recovering force to maintain the meniscus between the hammer handle and the

DOI: 10.1021/acs.jpcc.7b11123
J. Phys. Chem. C 2018, 122, 2747−2752

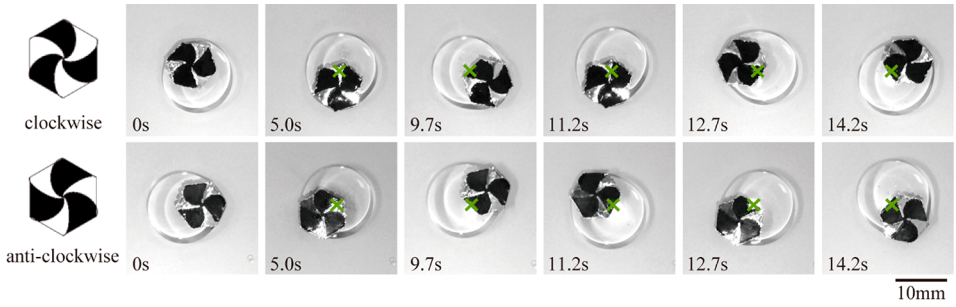

Figure 6. Clockwise and anticlockwise rotary motions with chiral propeller-shaped objects. The rotational direction is deterministic depending on the chirality of the Al object.

wall of the vessel due to interfacial tension, as shown schematically in Figure 3B. The last term on the first line of eq 1 is the driving force caused by the difference in interfacial tension, as shown in Figure 3B. The second differential equation in eq 1 describes the speed of the change in temperature around the hammer head caused by laser irradiation, where $\xi(\theta)$ is

$$\xi(\theta) = \begin{cases} 1 & 0 \le \theta < k \\ e^{-\eta(\theta-k)^2} & \theta \ge k \end{cases} \quad (2)$$

$\xi(\theta)$ expresses the efficiency of heating due to laser irradiation as a function of θ. Parameter k is a constant. The observed profile of $\xi(\theta)$ is depicted in Figure S2A and indicates that laser irradiation causes local heating only of the object itself. The steep decrease in heating efficiency in the region $\theta \ge k$ implies that the speed of heating decreases when the hammer-head part escapes from laser irradiation, as shown in Figure S2A. The effect of function $\xi(\theta)$ is explained in detail in Supplement 2.

Figures 4A and 4B exemplify the results of numerical calculations based on eqs 1 and 2, where we adopted $a = 0.241$, $b = 0.398$, $c = 0.315$, $e = 1.1$, $k = 0.25$, and $\eta = 7500$, where parameter a was determined from the decay of the angular velocity after sudden switch-off of the laser and parameter b was set so as to fit the periodicity of the rhythmic motion. Parameter e was estimated from the rate of decrease of temperature toward room temperature after switch-off of the laser under the condition that the hammer was spatially fixed. Parameter η was chosen so as to roughly fit the temperature profile near the edge of hammer as observed by the thermal camera. After setting these parameters, parameter c was chosen so as to reproduce the whole experimental trends in a similar manner. In relation to the procedure to find suitable parameters as explained above, we performed additional experiments to measure laser-induced escaping motion as shown in Supplement 1 and Figure S1. From such simple experimental system, it becomes possible to estimate the driving force and damping coefficient as in the phenomenological equation of motion as eq S1. When the laser power is weak, i.e., when d in eq 1 is small ($d = 0.3$), the calculated results indicated a damping motion of the object, which leads to a stationary state. On the other hand, the object exhibits limit-cycle behavior when d is sufficiently large ($d = 0.45$). Figure 4C shows the amplitude of the oscillatory motion depending on d in eq 1. Thus, the calculated results reproduce the essential features of the observed photoinduced pendular motion.

Next, we show the experimental results for the motion of a hexagonal Al sheet floating on a droplet of oleic acid, as shown in Figure 5A. A droplet of oleic acid (260 μL) was floated on an aqueous layer with a depth of ca. 5 mm in a container. Each side of the hexagonal Al sheet was 5 mm. Figure 5B shows the rotational motion of the Al sheet within the region of the oil droplet, under stationary laser irradiation with a power of 0.87 W. As shown in the lower part of Figure 5B, the Al sheet causes fluctuation within the oil droplet up to an induction period of ca. 5 s. Thereafter, the Al sheet exhibited continuous rotational motion around the laser spot. Figure 5C shows the results of the simultaneous observation of rotational motion with both a digital video camera and a thermal camera. The images show that there is a temperature difference between the front and rear of the hexagonal sheet as shown in the thermal images, with the corresponding position on the sheet marked with a green X. During rotational motion, the front part moves toward the laser spot and exhibits a gradual temperature increase. As a result, the degree of heating at the rear becomes significant, which causes a higher temperature at the rear than at the front. As in the experiments on pendular motion, the air/water interfacial tension at higher temperature becomes lower than that at lower temperature. Thus, during rotational motion, the hexagonal object continues to accept the driving force due to the difference in interfacial tension between the front and rear. Figure 5D shows the state of the hexagonal sheet depending on the laser power. Here again, similar to the pendular motion described above, the rotatory motion exhibits on/off switching depending on the laser power; i.e., the motion shows a subcritical-type transition. On the basis of the experimental results, we found that the direction of rotation of the object in the droplet is sensitive to the initial conditions; i.e., the direction of rotation is almost stochastic.

To develop a method for controlling the mode of rotation in a reliable manner, we performed experiments using an Al sheet with chiral asymmetry, as shown in Figure 6, where the Al sheet has a propeller-like morphology with chiral asymmetry. Using this chiral object, we succeeded in constructing an experimental system that undergoes directional rotation. The upper panels show the generation of clockwise rotation, and the bottom panels show anticlockwise rotation.

CONCLUSION

It has become clear that for a centimeter-sized metallic sheet floating on an aqueous solution, both stable pendular motion and rotary motion are generated under continuous photo-irradiation. The driving force is the spatial gradient of surface tension caused by photoabsorption on the metallic sheet. Interestingly, with a change in the color pattern on the sheet, rotational motion can become deterministic between clockwise and anticlockwise modes. It is expected that various regular motions besides simple pendular and rotational motion could

DOI: 10.1021/acs.jpcc.7b11123
J. Phys. Chem. C 2018, 122, 2747−2752

be realized through the suitable choice of morphology and the color pattern.

■ ASSOCIATED CONTENT

Supporting Information

The Supporting Information is available free of charge on the ACS Publications website at DOI: 10.1021/acs.jpcc.7b11123.

An experiment on the evaluation of actual driving force on an Al sheet floating on water surface under CW laser irradiation (Supplement 1, Figure S1) and additional numerical results on the transition from stationary onto rhythmic state (Supplement 2, Figure S2) (PDF)

Video S1: real-time observations on the pendular motion (AVI)

Video S2: real-time observations on the spontaneous rotary motion (AVI)

Video S3: real-time observations on the clockwise rotary motion (AVI)

Video S4: real-time observations on the anticlockwise rotary motion (AVI)

■ AUTHOR INFORMATION

Corresponding Author

*E-mail keyoshik@mail.doshisha.ac.jp; Ph +81-774-65-6243 (K.Y.).

ORCID

Kenichi Yoshikawa: 0000-0002-2751-7136

Author Contributions

Y.H., K.K., and H.S. contributed equally to this project. Y.H., K.K., H.S., and K.Y. conceived the project. Y.H., K.K., K.S., T.K., and K.Y. designed the experiments. Y.H. and K.K. performed most of the experimental work. H.S. and K.K. performed most of the numerical work. Y.H., H.S., and K.Y. wrote the manuscript. K.Y. provided supervision.

Notes

The authors declare no competing financial interest.

■ ACKNOWLEDGMENTS

This work was supported by JSPS KAKENHI Grants 15H02121, 25103012, 17K05615, 15K05400, and 16K13655.

■ REFERENCES

(1) Nakata, S.; Iguchi, Y.; Ose, S.; Kuboyama, M.; Ishii, T.; Yoshikawa, K. Self-Rotation of a Camphor Scraping on Water: New Insight into the Old Problem. *Langmuir* **1997**, *13*, 4454−4458.

(2) Julicher, F.; Kruse, K.; Prost, J.; Joanny, J. Active Behavior of the Cytoskeleton. *Phys. Rep.* **2007**, *449*, 3−28.

(3) Joanny, J. F.; Prost, J. Active Gels as a Description of the Actin-Myosin Cytoskeleton. *HFSP J.* **2009**, *3*, 94−104.

(4) Yoshikawa, K.; Magome, N. Chemomechanical Transduction in an Oil-Water System. Regulation of the Macroscopic Mechanical Motion. *Bull. Chem. Soc. Jpn.* **1993**, *66*, 3352−3357.

(5) Ramaswamy, S. The Mechanics and Statistics of Active Matter. *Annu. Rev. Condens. Matter Phys.* **2010**, *1*, 323−345.

(6) Marchetti, M. C.; Joanny, J. F.; Ramaswamy, S.; Liverpool, T. B.; Prost, J.; Rao, M.; Simha, R. A. Hydrodynamics of Soft Active Matter. *Rev. Mod. Phys.* **2013**, *85*, 1143−1189.

(7) Kümmel, F.; ten Hagen, B.; Wittkowski, R.; Buttinoni, I.; Eichhorn, R.; Volpe, G.; Löwen, H.; Bechinger, C. Circular Motion of Asymmetric Self-Propelling Particles. *Phys. Rev. Lett.* **2013**, *110*, 198302−198306.

(8) Loget, G.; Kuhn, A. Electric Field-Induced Chemical Locomotion of Conducting Objects. *Nat. Commun.* **2011**, *2*, 535−540.

(9) Chen, K.; Gu, C.; Yang, Z.; Nakajima, M.; Chen, T.; Fukuda, T. Z"-Shaped Rotational Au/Pt Micro-Nanorobot. *Micromachines* **2017**, *8*, 183−195.

(10) Ke, H.; Ye, S.; Carroll, R. L.; Showalter, K. Motion Analysis of Self-Propelled Pt−Silica Particles in Hydrogen Peroxide Solutions. *J. Phys. Chem. A* **2010**, *114*, 5462−5467.

(11) Elgeti, J.; Gompper, G. Microswimmers near Surfaces. *Eur. Phys. J.: Spec. Top.* **2016**, *225*, 2333−2352.

(12) Zhang, L.; Abbott, J. J.; Dong, L.; Peyer, K. E.; Kratochvil, B. E.; Zhang, H.; Bergeles, C.; Nelson, B. J. Characterizing the Swimming Properties of Artificial Bacterial Flagella. *Nano Lett.* **2009**, *9*, 3663−3667.

(13) Bechinger, C.; Di Leonardo, R.; Löwen, H.; Reichhardt, C.; Volpe, G.; Volpe, G. Active Particles in Complex and Crowded Environments. *Rev. Mod. Phys.* **2016**, *88*, 045006−045055.

(14) Dai, B.; Wang, J.; Xiong, Z.; Zhan, X.; Dai, W.; Li, C. C.; Feng, S. P.; Tang, J. Programmable Artificial Phototactic Microswimmer. *Nat. Nanotechnol.* **2016**, *11*, 1087−1092.

(15) Feldmann, D.; Maduar, S. R.; Santer, M.; Lomadze, N.; Vinogradova, O. I.; Santer, S. Manipulation of Small Particles at Solid Liquid Interface: Light Driven Diffusioosmosis. *Sci. Rep.* **2016**, *6*, 36443−36452.

(16) Shen, Z.; Su, L.; Yuan, X. C.; Shen, Y. C. Trapping and Rotating of a Metallic Particle Trimer with Optical Vortex. *Appl. Phys. Lett.* **2016**, *109*, 241901−241905.

(17) Lauga, E.; Davis, A. M. J. Viscous Marangoni Propulsion. *J. Fluid Mech.* **2012**, *705*, 120−133.

(18) Ichikawa, M.; Takabatake, F.; Miura, K.; Iwaki, T.; Magome, N.; Yoshikawa, K. Controlling Negative and Positive Photothermal Migration of Centimeter-Sized Droplets. *Phys. Rev. E* **2013**, *88*, 012403−012410.

(19) Takabatake, F.; Yoshikawa, K.; Ichikawa, M. Communication: Mode Bifurcation of Droplet Motion under Stationary Laser Irradiation. *J. Chem. Phys.* **2014**, *141*, 051103−051106.

(20) Dos Santos, F. D.; Ondarçuhu, T. Free-Running Droplets. *Phys. Rev. Lett.* **1995**, *75*, 2972−2975.

(21) Sumino, Y.; Magome, N.; Hamada, T.; Yoshikawa, K. Self-Running Droplet: Emergence of Regular Motion from Nonequilibrium Noise. *Phys. Rev. Lett.* **2005**, *94*, 068301−068304.

(22) Nagai, K. H.; Takabatake, F.; Sumino, Y.; Kitahata, H.; Ichikawa, M.; Yoshinaga, N. Rotational Motion of a Droplet Induced by Interfacial Tension. *Phys. Rev. E* **2013**, *87*, 013009−013013.

(23) Venancio-Marques, A.; Barbaud, F.; Baigl, D. Microfluidic Mixing Triggered by an External Led Illumination. *J. Am. Chem. Soc.* **2013**, *135*, 3218−3223.

(24) Suzuki, K.; Sugawara, T. Phototaxis of Oil Droplets Comprising a Caged Fatty Acid Tightly Linked to Internal Convection. *ChemPhysChem* **2016**, *17*, 2300−2303.

(25) Rybalko, S.; Magome, N.; Yoshikawa, K. Forward and Backward Laser-Guided Motion of an Oil Droplet. *Phys. Rev. E* **2004**, *70*, 046301−046304.

(26) Okawa, D.; Pastine, S. J.; Zettl, A.; Frechét, J. M. Surface Tension Mediated Conversion of Light to Work. *J. Am. Chem. Soc.* **2009**, *131*, 5396−5398.

(27) Delville, J.-P.; Robert de Saint Vincent, M.; Schroll, R. D.; Chraïbi, H.; Issenmann, B.; Wunenburger, R.; Lasseux, D.; Zhang, W. W.; Brasselet, E. Laser Microfluidics: Fluid Actuation by Light. *J. Opt. A: Pure Appl. Opt.* **2009**, *11*, 034015−034045.

(28) Horibe, N.; Hanczyc, M. M.; Ikegami, T. Mode Switching and Collective Behavior in Chemical Oil Droplets. *Entropy* **2011**, *13*, 709−719.

(29) Nagai, K. H.; Tachibana, K.; Tobe, Y.; Kazama, M.; Kitahata, H.; Omata, S.; Nagayama, M. Mathematical Model for Self-Propelled Droplets Driven by Interfacial Tension. *J. Chem. Phys.* **2016**, *144*, 114707−114714.

(30) Koyano, Y.; Gryciuk, M.; Skrobanska, P.; Malecki, M.; Sumino, Y.; Kitahata, H.; Gorecki, J. Relationship between the Size of a Camphor-Driven Rotor and Its Angular Velocity. *Phys. Rev. E: Stat.*

DOI: 10.1021/acs.jpcc.7b11123
J. Phys. Chem. C 2018, 122, 2747−2752

Phys., Plasmas, Fluids, Relat. Interdiscip. Top. **2017**, *96*, 012609−012616.
(31) Koyano, Y.; Yoshinaga, N.; Kitahata, H. General Criteria for Determining Rotation or Oscillation in a Two-Dimensional Axisymmetric System. *J. Chem. Phys.* **2015**, *143*, 014117−014122.
(32) Song, C.; Moon, J. K.; Lee, K.; Kim, K.; Pak, H. K. Breathing, Crawling, Budding, and Splitting of a Liquid Droplet under Laser Heating. *Soft Matter* **2014**, *10*, 2679−2684.

DOI: 10.1021/acs.jpcc.7b11123
J. Phys. Chem. C 2018, 122, 2747−2752